






Article

Features of the behavior of the barocaloric effect near ferroelectric phase transition close to the tricritical point

E.A. Mikhaleva ¹ , I.N. Flerov ^{1,2*} , M.V. Gorev ^{1,2} , V.S. Bondarev ^{1,2}  and E.V. Bogdanov ^{1,3} 

¹ Kirensky Institute of Physics, Federal Research Center KSC Siberian Branch, Russian Academy of Sciences, 660036 Krasnoyarsk, Russia; katerina@iph.krasn.ru (E.A.M.); flerov@iph.krasn.ru (I.N.F.); gorev@iph.krasn.ru (M.V.G.); vbondarev@yandex.ru (V.S.B.); evbogdanov@yandex.ru (E.V.B.)

² Institute of Engineering Physics and Radioelectronics, Siberian Federal University, 660074 Krasnoyarsk, Russia

³ Institute of Engineering Systems and Energy, Krasnoyarsk State Agrarian University, 660049 Krasnoyarsk, Russia

* Correspondence: flerov@iph.krasn.ru (I.N.F.)

Version December 24, 2019 submitted to Crystals

Abstract: A detailed study of the effect of temperature and pressure on heat capacity, entropy and hysteresis phenomena near the ferroelectric phase transition in ammonium sulfate (AS) was performed. An analysis of experimental results within the framework of the phenomenological theory showed that taking into account the temperature-dependent part of the anomalous entropy leads to a significant increase in the barocaloric effect (BCE). The maximum values of extensive and intensive BCE near the tricritical point are outstanding: $\Delta S_{BCE}^{max} \approx 85$ J/kgK, $\Delta T_{AD}^{max} \approx 12$ K and can be achieved at low pressure ~ 0.5 GPa.

Keywords: polymorphic phase transformation; phase diagram; order–disorder phenomena; entropy; barocaloric effect

1. Introduction

Solids showing significant caloric effects (CE) associated with the reversible change in the temperature, ΔT_{AD} , and entropy, ΔS_{CE} , under variation of the external field are considered as promising solid refrigerants in alternative cooling cycles [1–9].

Until recently, little attention was paid to the barocaloric effect (BCE) in ferroelectrics [10–14]. Nevertheless, it was found that even at low pressures the extensive, ΔS_{BCE} , and intensive, ΔT_{AD} , effects can significantly exceed the parameters of the electrocaloric effect realized in high electric fields [10,13,14].

The most impressive results are associated with BCE in ferroelectrics: $(\text{NH}_4)_2\text{SO}_4$ (AS), and NH_4HSO_4 (AHS) [11,15]. The main reason for the significant BCE near the first-order phase transitions $P_{nm} \leftrightarrow P_{na21}$ and $P_c \leftrightarrow P_1$ in AS and AHS, respectively, is due to the large values of entropy changes, ΔS_0 , and baric coefficients, dT/dp .

At the same time, the transformations in these compounds differ from each other by their closeness to the tricritical point characterized, in particular, by the relation between the jump in entropy, δS_0 , at the transition point, T_0 , and its total change, ΔS_0 . In accordance with the $\delta S_0/\Delta S_0$ values equal to 0.50 and 0.93 in AS and AHS, respectively, the phase transition in the former ferroelectric is significantly closer to tricritical point, where $\delta S_0/\Delta S_0 = 0$. Nevertheless, the value of δS_0 was found to be more sensitive to pressure in AHS, reaching zero at $p_{TCP} = 0.18$ GPa, while for AS this value is about 0.36 GPa.

29 Due to strong difficulties of the accurate measurements of the heat capacity of solids under
 30 pressure, the pressure dependencies of the temperature dependent anomalous entropy below the
 31 transition temperatures, $\Delta S(T, p) = \Delta S_0 - \delta S_0$, are unknown in AS [11] and AHS [15]. This is the
 32 reason why BCE in both ferroelectrics was determined without taking into account the dependencies
 33 $\Delta S_0(T, p)$ [11,15].

34 Recently, calorimetric studies of the AS powder sample were performed by differential scanning
 35 calorimeter (DSC) [11]. In this case, it is difficult to obtain reliable information about the heat capacity
 36 $C_p(T)$, entropy $S(T, p = 0)$ as well as their anomalous contributions associated with the phase
 37 transition. That is why the analysis of extensive BCE in AS was performed only taking into account
 38 the pressure dependences $T_0(p)$ and $\delta S_0(p)$ [11]. On the other hand, it is evidently that the behavior
 39 and maximum values of BCE should be strongly sensitive to the dependencies $S(T, p)$ and $\Delta S_0(T, p)$.

40 In the present paper, to get reliable information on the dependencies $C_p(T, p = 0)$, $S(T, p = 0)$,
 41 $\delta S_0(p)$ and $\Delta S_0(T, p = 0)$ and as result on the extensive and intensive BCE, we performed studies
 42 of single crystal AS using an adiabatic calorimeter as the most accurate and sensitive calorimetric
 43 method. Such measurements avoided distortion of the temperature dependence of the anomalous
 44 entropy and smearing of its jump which was determined by the method of quasistatic thermograms.
 45 On the same sample the pressure dependencies $T_0(p)$ and $\delta S_0(p)$ were determined using differential
 46 thermal analysis under pressure.

47 For phase transitions of the first order close to the tricritical point, the pressure behavior of both
 48 entropies can be restored analyzing the dependencies $S(T, p = 0)$, $\Delta S_0(T, p = 0)$, $\delta S_0(p)$ and $T_0(p)$
 49 in the framework of the Landau phenomenological theory [16–18]. Such an analysis is impossible
 50 for AHS due to the almost complete absence at atmospheric pressure of temperature-dependent
 51 anomalous heat capacity below the transition $Pc \leftrightarrow P1$ [19]. In the case of AS, the relatively small
 52 value of $\delta S_0/\Delta S_0$ and the wide temperature range of the existence of $\Delta S(T, p = 0)$ [11,20] suggest the
 53 applicability of the thermodynamic theory to the description of the transformation $Pnam \rightarrow Pna2_1$.

54 2. Experimental methods

55 AS single crystals were grown at 40 °C from an aqueous solution of powder AS. XRD examination
 56 showed an absence of the secondary phases and revealed an orthorhombic symmetry consistent with
 57 the space group $Pnam$ ($Z = 4$) with the expected lattice parameters [21].

58 Heat capacity measurements were performed on a single crystal with dimensions $5 \times 5 \times 2.5 \text{ mm}^3$
 59 by means of a homemade automated adiabatic calorimeter [22]. The inaccuracy in the heat capacity
 60 determination did not exceed (0.3–0.5)% over the whole temperature range investigated (80–280 K).
 61 Discrete and continuous heating was used to measure the heat capacity of the "sample + heater +
 62 contact grease" system. In the former case, the calorimetric step was varied from 0.5 to 3.0 K. In the
 63 latter case, the system was heated at rates $dT/dt = 0.1\text{--}0.3 \text{ K/min}$. The heat capacities of the heater and
 64 contact grease were determined in individual experiments.

65 Using home-made high-pressure chamber with multiplier [23], we performed differential thermal
 66 analysis (DTA) experiments to study the effect of hydrostatic pressure on temperature and entropy of
 67 the phase transition. Measurements were performed on a single crystal sample with dimensions of
 68 $2 \times 2 \times 2 \text{ mm}^3$. A pressure-transmitting medium was a mixture of silicon oil and pentane. In order
 69 to measure temperature T_0 and ΔC_p related to the phase transition, we used the copper–constantan
 70 and high-sensitive differential copper–germanium thermocouples, respectively. The pressure was
 71 measured by a manganin resistive sensor.

72 3. Results and discussion

73 The temperature dependence of the heat capacity $C_p(T)$ is shown in Figure 1(a). Anomaly
 74 associated with the phase transition was observed at $T_0 = 222.18 \pm 0.10 \text{ K}$. In the vicinity of T_0 ,
 75 investigations were carried out using a method of quasistatic thermograms with an average heating
 76 rate of $dT/dt = 6.5 \cdot 10^{-3} \text{ K/min}$. Figure 1(b) shows that the structural transformation is accompanied

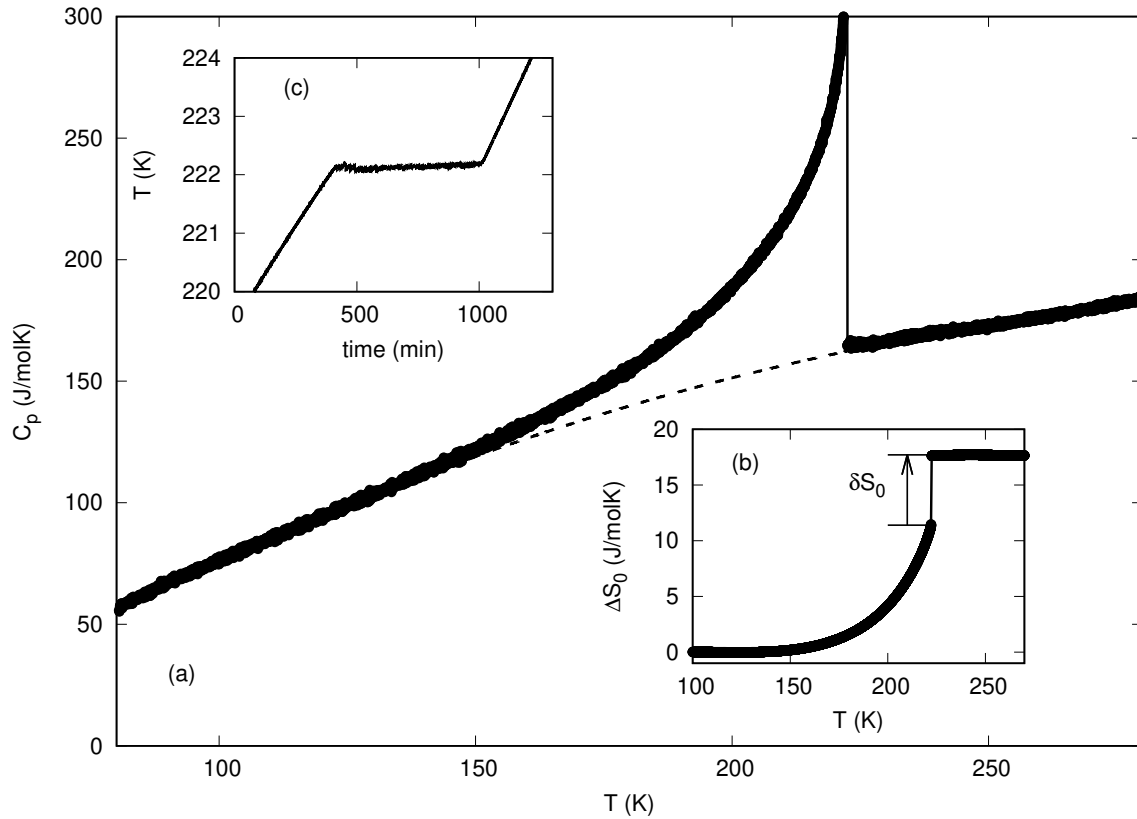


Figure 1. Temperature dependencies of (a) molar heat capacity and (b) anomalous entropy; (c) quasistatic thermogram near phase transition. The dashed line in (a) corresponds to the lattice heat capacity C_L .

77 by enthalpy jump $\delta H_0 = 1450 \pm 45$ J/mol without smearing due to the high quality of the single
78 crystal sample.

79 Information on the integral entropy change of the phase transition was obtained by separating the
80 anomalous, ΔC_p , and lattice, C_L , contributions to the total C_p using a simple model describing $C_L(T)$.
81 The experimental data taken far from the transition point ($T < 145$ K and $T > 230$ K) were fitted using
82 a linear combination of Debye and Einstein terms $C_L = K_D C_D + K_E C_E$, where

$$C_D(T) = 9R \left(\frac{T}{\Theta_D} \right)^3 \int_0^{\Theta_D/T} \frac{x^4 \exp(x)}{(\exp(x) - 1)^2} dx, \quad (1)$$

$$C_E(T) = 3R \left(\frac{\Theta_E}{T} \right)^2 \frac{\exp(\Theta_E/T)}{(\exp(\Theta_E/T) - 1)^2} \quad (2)$$

83 and K_D , K_E , Θ_D , Θ_E are fitting parameters. The average deviation of the experimental data from the
84 smoothed curve does not exceed 0.5%.

85 Figure 1(c) demonstrates the temperature behavior of entropy $\Delta S_0(T)$ associated with the phase
86 transition in AS. Its total value $\Delta S_0 = \int \Delta C_p/T = 17.7 \pm 0.8$ J/molK agrees well with the value
87 $3R \ln 2 = 17.3$ J/molK following from a model consideration of the $Pnam \leftrightarrow Pna2_1$ transition as an
88 order-disorder process [24]. The entropy jump at T_0 , $\delta S_0 = \delta H_0/T_0 = 6.5 \pm 0.2$ J/molK, is much
89 smaller than the value $\delta S_0 = 8.5$ J/molK determined by the less accurate DSC method [11].

90 Thus, in accordance with $\delta S_0/\Delta S_0 = 0.37$, the transition in single crystal AS is much closer to the
91 tricritical point in comparison with the powder sample ($\delta S_0/\Delta S_0 = 0.50$).

92 In order to determine the hysteresis corresponding to the equilibrium thermal conditions,
93 dependence of T_0 on the heating/cooling rate was studied in a wide range of the value $dT/dt =$

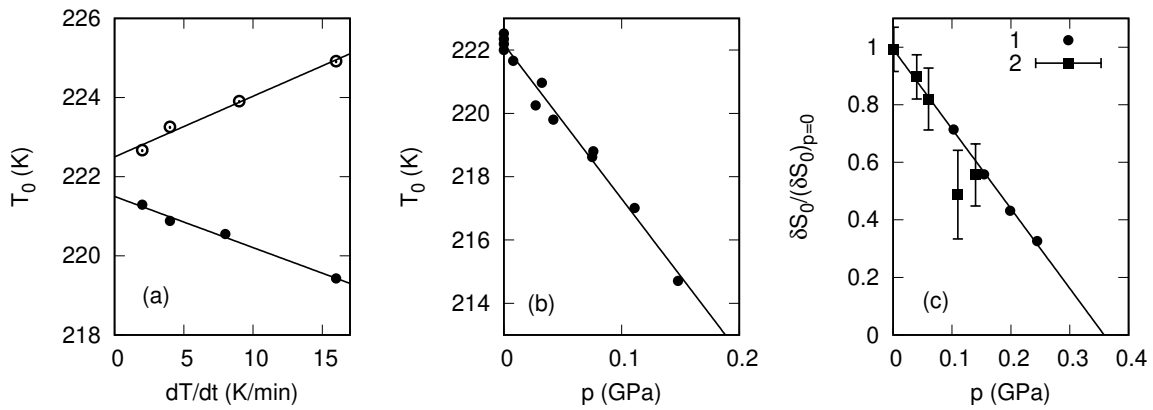


Figure 2. (a) Dependence of the phase transition temperature T_0 on the heating/cooling rate; (b) temperature-pressure phase diagram; (c) entropy jump δS_0 for the first order transition at different hydrostatic pressures.

94 $\pm(2 - 16)$ K/min using differential scanning microcalorimeter (Figure 2(a)). The dependencies
 95 $T_0 \uparrow (dT/dt)$ and $T_0 \downarrow (dT/dt)$ were found linear. At the rate of $dT/dt = \pm 8$ K/min, thermal
 96 hysteresis $\delta T_0 \approx 3.5$ K is comparable to value (3.5 K) obtained at a scanning rate ± 10 K/min [11].
 97 Extrapolation of the $T(dT/dt)$ dependencies to $dT/dt = 0$ allows one to obtain the real values of
 98 temperature of the phase transition $T_0 \uparrow = 222.5$ K, $T_0 \downarrow = 221.5$ K and a strong decrease in the thermal
 99 hysteresis $\delta T_0 = 1$ K.

100 At ambient pressure, the anomaly of DTA signal was detected at about $T_0 = 223 \pm 1$ K which
 101 agrees well with value observed during measurements of the heat capacity. Figure 2(b) shows that an
 102 increase in pressure is accompanied by linear decrease in T_0 with the rate $dT_0/dp = -49 \pm 3$ K/GPa
 103 which is close to the value for powder sample obtained in Ref. [11].

104 Due to the limited sensitivity of DTA, the area under the DTA peak at T_0 represents the enthalpy
 105 δH_0 (entropy δS_0) jump at T_0 . The value of δS_0 decreases with pressure and reaches zero at ~ 0.36 GPa
 106 that corresponds to the pressure of the tricritical point, p_{TCP} (Figure 2(c)). On the other hand, it is
 107 unlikely that such a low pressure may affect the degree of disordering of structural elements in initial
 108 phase $Pnam$ and as a result the total entropy change at the $Pnam \leftrightarrow Pna2_1$ transformation ΔS_0 remains
 109 constant.

110 Both BCE, ΔS_{BCE} and ΔT_{AD} , in AS could be determined by the previously used method [25]
 111 using data obtained in the present work on the heat capacity, $T - p$ phase diagram, and temperature
 112 and pressure dependencies of ΔS_0 and δS_0 , respectively. However, as mentioned above, it was first
 113 necessary to restore the temperature dependencies of the anomalous entropy at various pressures
 114 taking into account the relationship between ΔS_0 and the order parameter.

115 Despite the fact that polarization occurs during the phase transition in AS, there is no consensus
 116 on whether it is the main order parameter [18,26,27]. There are a number of models describing the
 117 phase transition in ammonium sulfate [18], but all of them do not fully take into account the interaction
 118 between the three types of tetrahedral groups and do not adequately describe the entire set of crystal
 119 properties based on the values of spontaneous deformation and polarization. For example, the model
 120 of an improper ferroelectric transition in AS [26] assumes that a certain parameter η is the main
 121 order parameter connected bilinearly with polarization which is not a critical parameter. Authors [26]
 122 introduce an ordering parameter η of some atoms along the ferroelectric axis, which does not contribute
 123 to the polarization but plays the role of a trigger for the occurrence of the spontaneous polarization,
 124 into the potential function

$$\Delta \Phi = \frac{1}{2} \alpha \eta^2 + \frac{1}{4} \gamma \eta^4 + \frac{1}{6} \delta \eta^6 + \frac{1}{2} \chi P^2 + f \eta P + \dots \quad (3)$$

125 As a result of a series of simple transformations, the potential (Equation 3) takes the following form

$$\Delta\Phi = A\eta^2 + B\eta^4 + C\eta^6, \quad (4)$$

126 where $A = A_T(T_0 - T_C) + A_T(T - T_0)$ and $T_C < T_0$ is the Curie temperature at which the inverse
127 susceptibility is zero.

In accordance with the equation of state, $\partial\Delta\Phi/\partial\eta = 0$, the temperature dependence of the order parameter is as follows

$$\eta^2 = [-B + (B^2 - 3AC)^{1/2}]/3C \quad (5)$$

128 and graphically in coordinates η^2 and (T) looks like a parabola.

Given the relation between the jump in the order parameter at T_0 and the coefficients in Equation 5

$$\eta_0^2 = -(B/2C) = -2A_T(T_0 - T_C)/B, \quad (6)$$

the equation of state (Equation 5) can be represented as convenient for the analysis of experimental data

$$[\eta^2 - (2/3)\eta_0^2]^2 = [(1/3)\eta_0^2]^2 + A_T(T_0 - T)/3C. \quad (7)$$

129 Here, the value $(2/3)\eta_0^2$ corresponds to the ordinate of the vertex of the parabola at T^* .

130 Analysis in the framework of thermodynamic theory can be performed taking into account the
131 relation between the order parameter and entropy, as well as their jumps [17,18]

$$\Delta S_0 = \partial\Delta\Phi/\partial T = A_T\eta^2; \quad \delta S_0 = A_T\eta_0^2. \quad (8)$$

132 Figure 3(a) shows that in a wide temperature range below T_0 at $p=0$, the dependence $\Delta S_0(T)$ is
133 quite satisfactorily described in the framework of the phenomenological theory with the following
134 parameters: $T^* \approx 223.1$ K, $T_C \approx 218.5$ K, $\delta S_0 \approx 6.3$ J/molK.

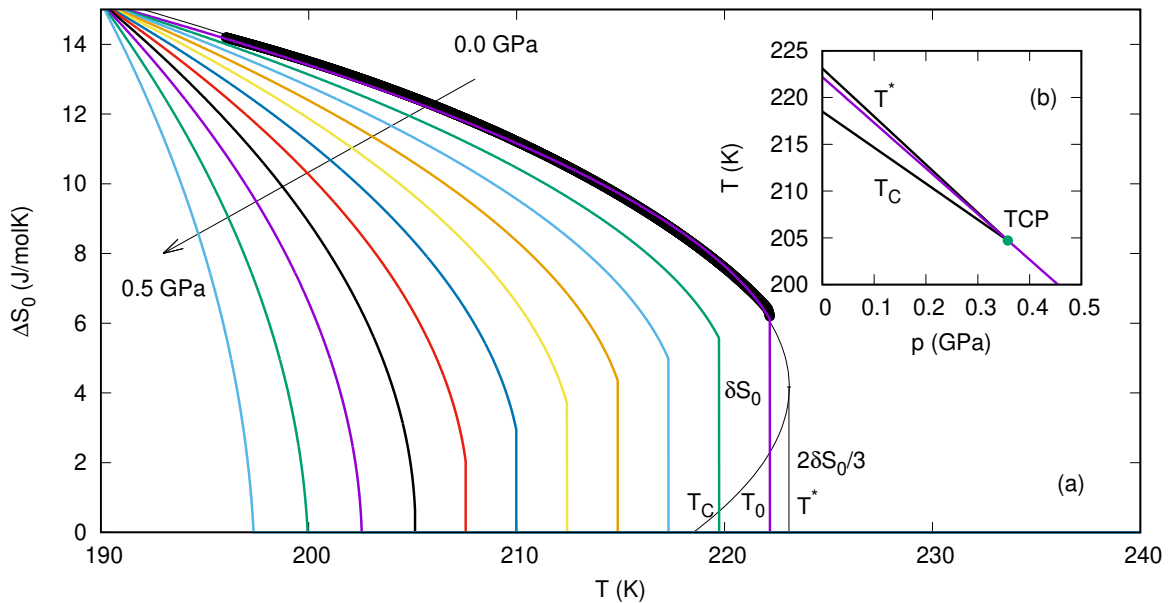


Figure 3. Temperature dependences of (a) anomalous entropy at various hydrostatic pressures; (b) refined $T - p$ phase diagram.

135 The behavior of the function $\Delta S_0(T)$ under pressure up to 0.5 GPa was restored taking into
136 account the dependencies $T_0(p)$ and $\delta S_0(p)$ (Figure 3(a)). In this case, the $T - p$ phase diagram
137 looks as shown in Figure 3(b). An increase in pressure leads to a decrease in the difference between
138 temperatures T^* and T_C , which become equal to T_0 at $p = p_{TCP}$. As result at $p > p_{TCP}$, AS undergoes

139 a second-order transformation close to the tricritical point. However, in this case too, the Equations 5,
140 6 and 7 remain valid for the analysis of the function $\Delta S_0(T)$ [16,17].

141 It was recently found that thermal expansion of the crystal lattice can play a significant role
142 in the formation of BCE [11,15,28]. Indeed, in accordance with Maxwell equation $(\partial S_L/\partial p)_T =$
143 $-(\partial V_L/\partial T)_p$ the lattice contribution to the isothermal entropy change is proportional to volumetric
144 thermal expansion coefficient β_L ,

$$\Delta S_L(T, p) = - \int_0^p (\partial V_L/\partial T)_p dp \approx -V_m \beta_L(T) p. \quad (9)$$

145 The molar volume, V_m , and $\beta_L(T)$ are weakly dependent on pressure, which was experimentally
146 established in Ref. [11].

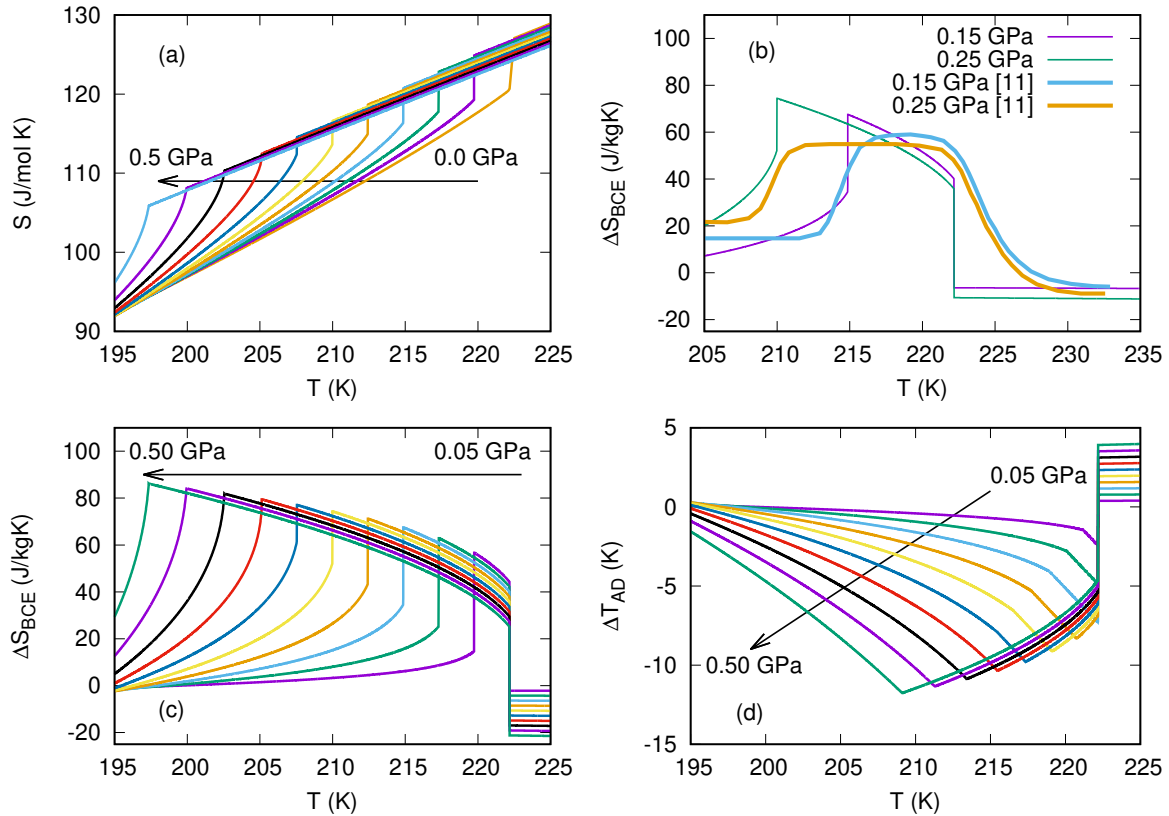


Figure 4. (a) Temperature dependencies of total entropy at different pressures; (b) comparison of extensive BCE obtained at $p \leq 0.25$ GPa in this paper and in Ref. [11]; behavior of (c) barocaloric entropy and (d) adiabatic temperature change at pressures up to 0.5 GPa.

147 Taking into account that AS is characterized by rather large positive value of $\beta_L(T) = (1.0 -$
148 $1.5)10^{-4} \text{ K}^{-1}$ [11], temperature dependencies of the total entropy under different pressures were
149 determined by summation of the lattice entropy, $S_L(T)$, and the anomalous contributions: $S(T, p) =$
150 $S_L(T, 0) + \Delta S_L(T, p) + \Delta S_0(T, p)$ (Figure 4(a)).

151 The extensive BCE was determined by analyzing the temperature dependencies of the total
152 entropy at different pressures: $\Delta S_{BCE} = S(T, p) - S(T, p = 0)$. Figure 4(b) shows the data obtained
153 in this paper and in Ref. [11] at relatively low pressures, $p \leq 0.25$ GPa. It can be seen that taking
154 into account the temperature-dependent part of the anomalous entropy correctly determined using
155 the adiabatic calorimeter leads to a significantly different behavior of $\Delta S_{BCE}(T)$ and to an increase
156 in its maximum value at the same pressure. Moreover, the restoration of the behavior of anomalous
157 entropy under pressure made it possible to analyze the dependencies $\Delta S_{BCE}(T)$ and $\Delta T_{AD}(T)$ at
158 pressures close to p_{TCP} and higher (Figures 4(c) and 4(d)). To obtain correct information on the

159 behavior of the intensive BCE, plots of $S(T, p)$ were analyzed based on the condition of constant
160 entropy $S(T, p) = S(T + \Delta T_{AD}, p = 0)$.

161 Due to the negative total coefficient β in the region of the phase transition and $\beta_L > 0$ [11], BCE in
162 AS consists of two contributions: inverse, $\Delta S_{BCE} > 0$, and conventional, $\Delta S_{BCE} < 0$, at $T < T_0$ and
163 $T > T_0$, respectively. This is the reason why the inverse extensive BCE cannot reach the maximum
164 value, which is equal to the total entropy of the phase transition. However, even at $p = 0.5$ GPa, the
165 maximum values of $\Delta S_{BCE}^{max} \approx 85$ J/kgK and $\Delta T_{AD}^{max} \approx 12$ K are significantly higher in comparison
166 with many materials undergoing phase transitions of various nature and considered as promising
167 solid-state refrigerants [1,3,7,8,11]. Moreover, Figure 4 shows that in accordance with Equation 9, the
168 jump of the conventional BCE associated with the contribution of the crystal lattice is proportional to
169 the pressure.

170 4. Conclusions

171 In conclusion, this letter demonstrates that the most correct information on BCE in materials
172 undergoing phase transitions close to the tricritical point can be achieved by using heat capacity
173 data obtained using adiabatic calorimeter. Analysis of these data for AS in the framework of the
174 phenomenological theory, together with the dependencies $T(p)$, $\delta S(p)$, $T(dT/dt)$ determined in this
175 paper, allowed: 1) to restore the magnitude and behavior under pressure of the entropy associated with
176 the phase transition; 2) to build a detailed $T - p$ phase diagram showing the behavior of characteristic
177 temperatures: T^* , T_C and T_0 and, as a result, a change in hysteresis phenomena under pressure up
178 to the tricritical point. It was shown that taking into account the temperature dependent anomalous
179 entropy leads to a strong increase in the maximum values of ΔS_{BCE}^{max} and ΔT_{AD}^{max} , as well as to a
180 significant change in the temperature and pressure dependences of extensive and intensive BCE as
181 compared to the case when only the behavior of the entropy jump was analyzed[11]. Even at low
182 pressure $p \leq 0.5$ GPa, AS demonstrates BCE parameters that are comparable and/or even exceed the
183 same parameters for materials considered to be promising solid-state refrigerants [1,3,7,8,11].

184 **Author Contributions:** Investigation, V.S.B and E.V.B; Conceptualization, I.N.F.; Formal analysis, E.A.M.; Writing
185 – Original draft preparation, M.V.G.

186 **Funding:** The reported study was supported by the Russian Science Foundation (Project no.19-72-00023).

187 **Conflicts of Interest:** The authors declare no conflict of interest.

188 Abbreviations

189 The following abbreviations are used in this manuscript:

190 AS	ammonium sulfate
191 BCE	barocaloric effect
DTA	differential thermal analysis

192 References

- 193 1. Gschneidner Jr, K. A.; Pecharsky, V. K.; Tsokol, A. O. Recent developments in magnetocaloric materials *Rep.*
194 *Prog. Phys.* **2005**, *68*, 1479-1539.
- 195 2. Brown, J. S.; Domanski, P. A. Review of alternative cooling technologies. *Applied Thermal Engineering* **2014**,
196 *64*, 252 – 262.
- 197 3. Moya, X.; Kar-Narayan, S.; Mathur, N. D. Caloric materials near ferroic phase transitions. *Nat. Mater.* **2014**,
198 *13*, 439–450.
- 199 4. Plaznik, U.; Vrabelj, M.; Kutnjak, Z.; Malič, B.; Poredoš, A.; Kitanovski, A. Electrocaloric cooling: The
200 importance of electric-energy recovery and heat regeneration. *Europhysics Letters* **2015**, *111*, 57009.
- 201 5. Kitanovski, A.; Plaznik, U.; Tomc, U.; Poredoš, A. Present and future caloric refrigeration and heat-pump
202 technologies. *Int. J. Refrigeration* **2015**, *57*, 288 – 298.

- 203 6. Liu, Y.; Scott, J. F.; Dkhil, B. Some strategies for improving caloric responses with ferroelectrics. *APL Materials*
204 **2016**, *4*, 064109.
- 205 7. Mañosa, L.; Planes, A. Materials with giant mechanocaloric effects: Cooling by strength. *Adv. Mater.* **2017**,
206 *29*, 1603607.
- 207 8. Zarkevich, N. A.; Johnson, D. D.; Pecharsky, V. K. High-throughput search for caloric materials: the
208 CaloriCool approach. *J. Phys. D: Appl. Phys.* **2017**, *51*, 024002.
- 209 9. Michaelis, N.; Welsch, F.; Kirsch, S.-M.; Schmidt, M.; Seelecke, S.; Schütze, A. Experimental parameter
210 identification for elastocaloric air cooling. *Int. J. Refrigeration* **2019**, *100*, 167 – 174.
- 211 10. Mikhaleva, E. A.; Flerov, I. N.; Gorev, M. V.; Molokeev, M. S.; Cherepakhin, A. V.; Kartashev, A. V.;
212 Mikhashenok, N. V.; Sablina, K. A. Caloric characteristics of PbTiO₃ in the temperature range of the
213 ferroelectric phase transition. *Phys. Solid State* **2012**, *54*, 1832–1840.
- 214 11. Lloveras, P.; Stern-Taulats, E.; Barrio, M.; Tamarit, J.-L.; Crossley, S.; Li, W.; Pomjakushin, V.; Planes, A.;
215 Mañosa, L.; Mathur, N. D.; Moya, X. Giant barocaloric effects at low pressure in ferroelectric ammonium
216 sulphate. *Nat. Commun.* **2015**, *6*, 8801.
- 217 12. Khassaf, H.; Patel, T.; Alpay, S. P. Combined intrinsic elastocaloric and electrocaloric properties of
218 ferroelectrics. *J. Appl. Phys.* **2017**, *121*, 144102.
- 219 13. Liu, Y.; Wei, J.; Janolin, P.-E.; Infante, I. C.; Lou, X.; Dkhil, B. Giant room-temperature barocaloric effect and
220 pressure-mediated electrocaloric effect in BaTiO₃ single crystal. *Appl. Phys. Lett.* **2014**, *104*, 162904.
- 221 14. Mikhaleva, E. A.; Flerov, I. N.; Bondarev, V. S.; Gorev, M. V.; Vasiliev, A. D.; Davydova, T. N. Electrocaloric
222 and barocaloric effects in some ferroelectric hydrosulfates and triglycinesulfate. *Ferroelectrics* **2012**, *430*,
223 78–83.
- 224 15. Gorev, M. V.; Mikhaleva, E. A.; Flerov, I. N.; Bogdanov, E. V. Conventional and inverse barocaloric effects in
225 ferroelectric NH₄HSO₄. *J. Alloys and Compounds* **2019**, *806*, 1047 – 1051.
- 226 16. Landau, L. D.; Lifshitz, E. M. *Statistical Physics*, 3rd Edition, Vol. 5; Butterworth-Heinemann, 1980.
- 227 17. Aleksandrov, K. S.; Flerov, I. N. Ranges of applicability of thermodynamic theory of structural phase
228 transitions near the tricritical point. *Sov. Phys. Solid State* **1979**, *21*, 195–200.
- 229 18. Aleksandrov, K. S.; Beznosikov, B. V. *Strukturnye fazovye perekhody v kristallakh (Semeistvo sulfata kaliya)*;
230 Novosibirsk: Nauka, 1993.
- 231 19. Mikhaleva, E.; Flerov, I.; Kartashev, A.; Gorev, M.; Bogdanov, E.; Bondarev, V. Thermal, dielectric and
232 barocaloric properties of NH₄HSO₄ crystallized from an aqueous solution and the melt. *Solid State Sciences*
233 **2017**, *67*, 1–7.
- 234 20. Hoshino, S.; Vedam, K.; Okaya, Y.; Pepinsky, R. Dielectric and thermal study of (NH₄)₂SO₄ and (NH₄)₂BeF₄
235 transitions. *Phys. Rev.* **1958**, *11*, 405–412.
- 236 21. Shmyt'ko, I. M.; Afonikova, N. S.; Torgashev, V. I. Anomalous states of the structure of (NH₄)₂SO₄ crystals in
237 the temperature range 4.2–300 K. *Phys. Solid State* **2002**, *44*, 2309–2317.
- 238 22. Kartashev, A. V.; Flerov, I. N.; Volkov, N. V.; Sablina, K. A. Adiabatic calorimetric study of the intense
239 magnetocaloric effect and the heat capacity of (La_{0.4}Eu_{0.6})_{0.7}Pb_{0.3}MnO₃. *Phys. Solid State* **2008**, *50*, 2115–2120.
- 240 23. Flerov, I. N.; Gorev, M. V.; Fokina, V. D.; Bovina, A. F.; Laptash, N. M. Calorimetric and X-ray diffraction
241 studies of the (NH₄)₃WO₃F₃ and (NH₄)₃TiOF₅ perovskite-like oxyfluorides. *Physics of the Solid State* **2004**,
242 *46*, 915–921.
- 243 24. O'Reilly, D. E.; Tsang, T. Order–disorder transition in ferroelectric ammonium sulfate. *The Journal of Chemical*
244 *Physics* **1969**, *50*, 2274–2275.
- 245 25. Gorev, M. V.; Flerov, I. N.; Bogdanov, E. V.; Voronov, V. N.; Laptash, N. M. Barocaloric effect near the
246 structural phase transition in the Rb₂KTiOF₅ oxyfluoride. *Phys. Solid State* **2010**, *52*, 377–383.
- 247 26. Kobayashi, J.; Enomoto, Y.; Sato, Y. A phenomenological theory of dielectric and mechanical properties of
248 improper ferroelectric crystals. *Phys. Stat. Solidi (b)* **1972**, *50*, 335–343.
- 249 27. Romanyuk, N. A.; Gaba, V. M.; Ursul, Z. M. Optic and temperature anomalies of ammonium sulfate in phase
250 transitions. *Ukr. Fiz. Zh.* **1988**, *33*, 1381–1388.
- 251 28. Flerov, I.; Gorev, M.; Kartashev, A.; Pogorel'tsev, E.; Laptash, N. Heat capacity, thermal expansion and
252 barocaloric effect in fluoride K₂TaF₇. *J. Mat. Sci.* **2019**, *54*, 14287–14295.